

Physics-model-guided Worst-case Sampling for Safe Reinforcement Learning

Hongpeng Cao
 Technical University of Munich
 Munich, Germany
 cao.hongpeng@tum.de

Lui Sha
 University of Illinois Urbana-Champaign
 Urbana, USA
 lrs@illinois.edu

Yanbing Mao
 Wayne State University
 Detroit, USA
 hm9062@wayne.edu

Marco Caccamo
 Technical University of Munich
 Munich, Germany
 mcaccamo@tum.de

Abstract

Real-world accidents in learning-enabled CPS frequently occur in challenging corner cases. During the training of deep reinforcement learning (DRL) policy, the standard setup for training conditions is either fixed at a single initial condition or uniformly sampled from the admissible state space. This setup often overlooks the challenging but safety-critical corner cases. To bridge this gap, this paper proposes a physics-model-guided worst-case sampling strategy for training safe policies that can handle safety-critical cases toward guaranteed safety. Furthermore, we integrate the proposed worst-case sampling strategy into the physics-regulated deep reinforcement learning (Phy-DRL) framework to build a more data-efficient and safe learning algorithm for safety-critical CPS. We validate the proposed training strategy with Phy-DRL through extensive experiments on a simulated cart-pole system, a 2D quadrotor, a simulated and a real quadruped robot, showing remarkably improved sampling efficiency to learn more robust safe policies.

CCS Concepts

• **Computing methodologies** → **Computational control theory**.

Keywords

Safety Critical Systems, Worst Case Sampling, Safe Deep Reinforcement Learning

ACM Reference Format:

Hongpeng Cao, Yanbing Mao, Lui Sha, and Marco Caccamo. 2025. Physics-model-guided Worst-case Sampling for Safe Reinforcement Learning. In *Proceedings of ACM Conference (ICCPs '25)*. ACM, New York, NY, USA, 10 pages. <https://doi.org/XXXXXXX.XXXXXXX>

Permission to make digital or hard copies of all or part of this work for personal or classroom use is granted without fee provided that copies are not made or distributed for profit or commercial advantage and that copies bear this notice and the full citation on the first page. Copyrights for components of this work owned by others than the author(s) must be honored. Abstracting with credit is permitted. To copy otherwise, or republish, to post on servers or to redistribute to lists, requires prior specific permission and/or a fee. Request permissions from permissions@acm.org.
ICCPs '25, June 03–05, 2025, Woodstock, NY

© 2025 Copyright held by the owner/author(s). Publication rights licensed to ACM.
 ACM ISBN 978-1-4503-XXXX-X/18/06
<https://doi.org/XXXXXXX.XXXXXXX>

1 Introduction

Deep reinforcement learning (DRL) has been integrated into many cyber-physical systems (CPS; see examples in Figure 1), defining learning-enabled CPS that have succeeded tremendously in many complex control tasks. Notable examples range from autonomous driving [25, 26] to chemical processes [19, 40] to robot locomotion [22, 28]. Learning-enabled CPS promise to revolutionize many processes in different industries with tangible economic impact [33, 42]. However, the public-facing AI incident database [1] reveals that machine learning (ML) techniques, including DRL, can deliver much high performance but no safety assurance [48]. For instance, in 2023, the US NHTSA reported nearly 224 crashes linked to self-driving and driver-assist technologies within a 9-month period [36]. Hence, a high-performance DRL with enhanced safety assurance is even more vital today, aligning well with the market's need for ML safety.

1.1 Related Work on Safe DRL

To train a safe DRL policy, many literature adopts a constrained Markov decision process (CMDP) formulation, aiming to find a policy that jointly optimizes the objective of increasing the accumulated reward and decreasing the cost of safety violation [2, 29, 43]. Furthermore, incorporating safety knowledge into the reward function design incentivizes the DRL to learn a safe policy. For instance, the control Lyapunov function (CLF) is widely used in constructing the safety-embedded reward [3, 11, 37, 49]. However, the safety of those learned policies can not be formally guaranteed due to the neural network parameterized policy, whose behaviors are hard to predict [20] and verify [24].

Instead of focusing on learning a safe policy, the system-level safety framework sandboxes the unverified potential unsafe DRL policies regardless of the concrete design of the learning algorithm, and the safety is assured by an external verified safety controller [8, 14, 21, 45, 50]. However, those frameworks are often sensitive to the changes of the assumed dynamics models during the deployment.

Moreover, another focus of safe DRL has been shifted to integrating data-driven DRL action policy and physics-model-based action policy, leading to a residual action policy diagram [12, 13, 23, 30, 38]. However, the physics models considered in those works are nonlinear and intractable, which thwarts delivering a verifiable safety, if not impossible. Recently, a physics-regulated deep reinforcement

learning (Phy-DRL) framework [9, 10] is proposed to offer a promising solution to these challenges. Phy-DRL allows for the simplification of nonlinear system dynamics models into analyzable and verifiable linear models, which delivers a mathematically provable safety guarantee. Moreover, these linear models can then guide the construction of safety-embedded rewards and residual action policies.

Nevertheless, in the aforementioned safe DRL frameworks, the policy learning setup is often fixed at a single initial condition or uniformly sampled from the admissible state space [9, 10, 12, 13, 23, 27, 30, 32, 35, 38, 39], which overlooks the challenging but safety-critical corner cases, potentially leading an unsafe policy.

1.2 Open Problems

In particular, incidents of learning-enabled CPS (e.g., self-driving cars) often occur in infrequent corner cases [5, 6, 51]. This underscores that “corner cases” induce a formidable safety challenge for DRL and other ML techniques. From a control-theoretic perspective, system-state samples close to the safety boundary represent the corner cases where a slight disturbance or fault can take a system out of control. Intuitively, focusing the training on such corner-case samples will enable a more robust and safe action policy. In the safe DRL community, how to define those corner cases and how to use them for learning safe policies remains unclear.

1.3 Core Contributions

To bridge the gap of training on corner cases in the existing literature, we propose a formal definition of the worst case for DRL based on the system’s dynamics model. Furthermore, we propose an algorithm to efficiently generate the worst cases for policy learning. At last, we integrate the worst-case sampling into the Phy-DRL framework to learn safer and more robust policies. As shown in Figure 1, the integrated Phy-DRL framework defines worst-case samples as the state of the system located on the boundary of a safety envelope. These corner-case samples are not often visited during training via random sampling. Worst-case sampling thus lets Phy-DRL’s training focus on the safety boundary, enabling a more robust and safe action policy. We demonstrate the worst-case empowered Phy-DRL in three case studies including a cart-pole system, a 2D quadrotor, and a quadruped robot, showing remarkable improvement in sampling efficiency and safety assurance.

Table 1: Notations throughout Paper

\mathbb{R}^n	set of n -dimensional real vectors
\mathbb{N}	set of natural numbers
$[\mathbf{x}]_i$	i -th entry of vector \mathbf{x}
$[\mathbf{W}]_{i,:}$	i -th row of matrix \mathbf{W}
$[\mathbf{W}]_{i,j}$	matrix \mathbf{W} ’s element at row i and column j
$\mathbf{P} > (<) 0$	matrix \mathbf{P} is positive (negative) definite
\top	matrix or vector transposition
$ \cdot $	set cardinality, or absolute value
\mathbf{I}_n	n -dimensional identity matrix
$\mathbb{X} \setminus \Omega$	complement set of Ω with respect to \mathbb{X}

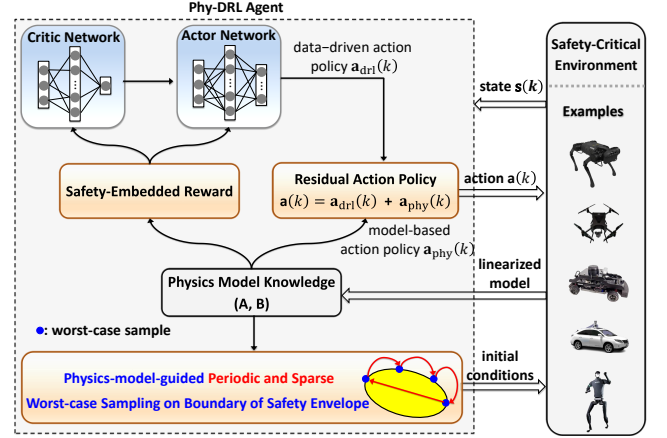


Figure 1: Phy-DRL training powered by periodic and sparse worst-case sampling for safety-critical CPS.

2 Preliminaries

2.1 Notations

We summarize notations used through the paper in Table 1

2.2 Safety Definition

The dynamics model of a real plant can be described by

$$\mathbf{s}(k+1) = \mathbf{A} \cdot \mathbf{s}(k) + \mathbf{B} \cdot \mathbf{a}(k) + \mathbf{f}(\mathbf{s}(k), \mathbf{a}(k)), \quad k \in \mathbb{N} \quad (1)$$

where $\mathbf{f}(\mathbf{s}(k), \mathbf{a}(k)) \in \mathbb{R}^n$ is the unknown model mismatch, $\mathbf{A} \in \mathbb{R}^{n \times n}$ and $\mathbf{B} \in \mathbb{R}^{n \times m}$ denote known system matrix and control structure matrix, respectively, $\mathbf{s}(k) \in \mathbb{R}^n$ is system state, $\mathbf{a}(k) \in \mathbb{R}^m$ is action. The available knowledge of the model related to the real plant (1) is represented by (\mathbf{A}, \mathbf{B}) . We are interested in an action policy that can constrain the system states to the safety set \mathbb{X} :

$$\mathbb{X} \triangleq \left\{ \mathbf{s} \in \mathbb{R}^n \mid \underline{\mathbf{v}} \leq \mathbf{D} \cdot \mathbf{s} - \mathbf{v} \leq \bar{\mathbf{v}}, \mathbf{D} \in \mathbb{R}^{h \times n}, \text{ with } \mathbf{v}, \bar{\mathbf{v}}, \underline{\mathbf{v}} \in \mathbb{R}^h \right\}, \quad (2)$$

where \mathbf{D} , \mathbf{v} , $\bar{\mathbf{v}}$ and $\underline{\mathbf{v}}$ are given in advance for formulating $h \in \mathbb{N}$ safety conditions. To guarantee the system always stays in the safety set, we introduce a subset of the safety set \mathbb{X} called safety envelope Ω based on *Lyapunov-stability theorem*.

$$\text{Safety Envelope } \Omega \triangleq \left\{ \mathbf{s} \in \mathbb{R}^n \mid \mathbf{s}^\top \cdot \mathbf{P} \cdot \mathbf{s} \leq 1, \mathbf{P} > 0 \right\}, \quad (3)$$

where $\mathbf{P} \in \mathbb{R}^{n \times n}$ is a positive definite matrix, that defines the shape of Ω . With the safety envelope Ω , the safety problem is defined as the follows:

Definition 2.1. [10] Consider the safety set \mathbb{X} (2) and the safety envelop Ω (3). The real plant (1) is said to be safe, if given any $\mathbf{s}(1) \in \Omega \subseteq \mathbb{X}$, the $\mathbf{s}(k) \in \Omega \subseteq \mathbb{X}$ holds for any time $k \in \mathbb{N}$.

To guarantee a system controlled by a DRL agent staying in the safety envelope Ω is non-trivial due to its unverifiable action output. The recent literature Phy-DRL [10] suggests that incorporating the knowledge of the physics model into the standard DRL framework can significantly improve safety assurance toward guaranteed safety. We summarize the Phy-DRL framework in the next section.

2.3 Phy-DRL Agent

Phy-DRL is built on the deterministic policy algorithms [16, 31]. As shown in Figure 1, its control action is in residual form:

$$\mathbf{a}(k) = \underbrace{\mathbf{a}_{\text{drl}}(k)}_{\text{data-driven}} + \underbrace{\mathbf{a}_{\text{phy}}(k) (:= \mathbf{F} \cdot \mathbf{s}(k))}_{\text{model-based}}, \quad (4)$$

where $\mathbf{a}_{\text{drl}}(k)$ denotes a data-driven action from DRL, while $\mathbf{a}_{\text{phy}}(k)$ is a model-based action. Meanwhile, Phy-DRL embeds safety envelope (3) into reward design, creating safety-embedded reward:

$$\begin{aligned} \mathcal{R}(\mathbf{s}(k), \mathbf{a}_{\text{drl}}(k)) & \quad (5) \\ &= \underbrace{\mathbf{s}^\top(k) \cdot \mathbf{H} \cdot \mathbf{s}(k) - \mathbf{s}^\top(k+1) \cdot \mathbf{P} \cdot \mathbf{s}(k+1)}_{\triangleq c(\mathbf{s}(k), \mathbf{s}(k+1))} + w(\mathbf{s}(k), \mathbf{a}(k)), \end{aligned}$$

where the term $w(\mathbf{s}(k), \mathbf{a}(k))$ aims at high-performance operations (e.g., minimizing energy consumption of resource-limited robots [18, 46]). The term $c(\mathbf{s}(k), \mathbf{s}(k+1))$ is safety-critical, in which

$$\mathbf{H} \triangleq \bar{\mathbf{A}}^\top \cdot \mathbf{P} \cdot \bar{\mathbf{A}}, \text{ with } \bar{\mathbf{A}} \triangleq \mathbf{A} + \mathbf{B} \cdot \mathbf{F} \text{ and } 0 < \mathbf{H} < \alpha \cdot \mathbf{P}, \alpha \in (0, 1), \quad (6)$$

where α is a pre-defined parameter to determine the decrease rate of the Lyapunov value. The matrix \mathbf{P} is the matrix for building the safety envelope Ω (3) and \mathbf{F} is the feedback control law. With the available physics-model knowledge (\mathbf{A}, \mathbf{B}) at hand, the \mathbf{F} and \mathbf{P} can be computed using LMI toolbox [7, 17]. We refer interested readers to [10] for a more detailed explanation of LMI formulations. The intuition of the sub-reward $c(\mathbf{s}(k), \mathbf{s}(k+1))$ is that we encourage the DRL agent to learn a safe policy in conjunction with the model-based policy a_{phy} to stabilize the real plant (1) toward the equilibrium point.

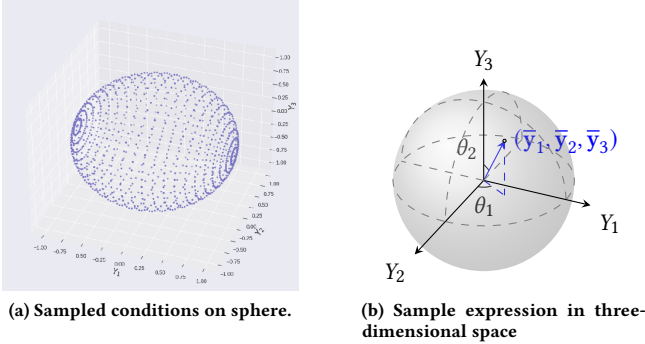


Figure 2: Worst-case condition generation in for a three-dimensional ($n = 3$) safety envelope.

3 Worst-case Sampling for Phy-DRL Training

The safety envelope is centered at the control equilibrium point. The plant is more likely to violate the safety constraint when its state is near the envelope boundary. For a DRL-controlled system, it is hard to certify and predict the output of the DRL output due to its non-convexity and non-linearity. Therefore, ensuring the safety of the DRL at the boundary of the envelope is critical. In this section, we propose a definition of the worst conditions for DRL in

a safety-critical system and a practical algorithm to generate these conditions for DRL training and testing.

Definition 3.1 (Worst-case conditions). Referring to the safety envelop in Equation (3), a state \mathbf{s} is said to be a worst-case condition if $\mathbf{s}^\top \cdot \mathbf{P} \cdot \mathbf{s} = 1$ (i.e., locating on the boundary of safety envelope).

Recall that, given n dimensional safety constraints, the solution for the safety envelope becomes a n dimensional hyperellipsoid, to generate worst-case samples referring to Definition 3.1, we need to solve $\mathbf{s}^\top \cdot \mathbf{P} \cdot \mathbf{s} = 1$, where $\mathbf{s} \in \mathbb{R}^n$. To achieve this, we present the following lemma for having explicit solutions of worst-case conditions.

Lemma 3.2. Given $\mathbf{P} > 0$, the solution of $\mathbf{s} \in \mathbb{R}^n$, being subject to $\mathbf{s}^\top \cdot \mathbf{P} \cdot \mathbf{s} = \varphi$, is

$$\mathbf{s} = \mathbf{Q}(\mathbf{P}) \cdot \mathbf{y}, \text{ with } [\mathbf{y}]_i = \begin{cases} \sqrt{\frac{\varphi}{\lambda_i(\mathbf{P})}} \cdot \sin(\theta_1) \cdot \prod_{m=2}^{n-1} \sin(\theta_m), & i = 1 \\ \sqrt{\frac{\varphi}{\lambda_i(\mathbf{P})}} \cdot \cos(\theta_{i-1}) \cdot \prod_{m=i}^{n-1} \sin(\theta_m), & i \geq 2 \end{cases} \quad (7)$$

where $\mathbf{Q}(\mathbf{P})$ is \mathbf{P} 's orthogonal matrix, and $\lambda_i(\mathbf{P})$ is the i -th eigenvalue of matrix $\mathbf{P} \in \mathbb{R}^{n \times n}$.

PROOF. See Appendix A.2. \square

Example in 3D case: Consider a three-dimensional safety envelop, i.e., $\mathbf{s} \in \mathbb{R}^3$. In this example, according to Equation (21), we have

$$\sum_{i=1}^3 \frac{\lambda_i(\mathbf{P})}{\varphi} \cdot \mathbf{y}_i^2 = 1, \mathbf{y} = \mathbf{Q}^\top(\mathbf{P}) \cdot \mathbf{s} \quad (8)$$

for which we define

$$\bar{\mathbf{y}}_i \triangleq \sqrt{\frac{\lambda_i(\mathbf{P})}{\varphi}} \cdot \mathbf{y}_i, \quad (9)$$

in light of (9), Equation (8) can be rewritten as

$$\bar{\mathbf{y}}_1^2 + \bar{\mathbf{y}}_2^2 + \bar{\mathbf{y}}_3^2 = 1, \quad (10)$$

which describes a sphere in \mathbb{R}^3 space, as shown in Figure 2 (a). From Figure 2 (b), we notice that every point on the sphere can be parameterized using angles θ_1 and θ_2 as:

$$\bar{\mathbf{y}}_i \triangleq \begin{cases} \sin(\theta_2) \cdot \sin(\theta_1), & i = 1 \\ \sin(\theta_2) \cdot \cos(\theta_1), & i = 2 \\ \cos(\theta_2), & i = 3. \end{cases} \quad (11)$$

By selecting different values for θ_1 and θ_2 , we can sample any point $[\bar{\mathbf{y}}_1, \bar{\mathbf{y}}_2, \bar{\mathbf{y}}_3]^\top$ on the sphere and, consequently, obtain the conditions on the boundary of the safety envelop (indicated by Equation (8) and Equation (9))

We now are ready to propose an algorithm to automatically generate sampling conditions located at the safety envelope's boundary. Moreover, we design a training curriculum to periodically visit the worst-case conditions for policy learning.

As shown in Algorithm 1, the proposed algorithm includes worst-case condition generation Line 3–Line 15, and training curriculum Line 16 – Line 21. In worst-case condition generation, we sample $\theta_1, \theta_2, \dots, \theta_{n-1}$ sparsely in the interval $[0, 2\pi)$. This is motivated

Algorithm 1 Periodic and Worst-case Sampling for Phy-DRL Training

```

1: Input: System-state dimension  $n \in \mathbb{N}$ ; sample numbers  $\bar{q}_r \in \mathbb{N}$ ,  $r = 1, \dots, n-1$ ; matrix  $\mathbf{P}$ ; parameter  $\varphi = 1$ , Period number  $p \in \mathbb{N}$ .
2: Initialize boundary set:  $\mathbb{B}_\varphi^{\mathbf{P}} \leftarrow \emptyset$ ;
3: for  $\theta_1 = 0 : \frac{2\pi}{\bar{q}_1} : (2\pi - \frac{2\pi}{\bar{q}_1})$  do ▷ Generating worst-case conditions
4:   Set:  $\theta_2 \leftarrow 0, \theta_3 \leftarrow 0, \dots, \theta_{n-1} \leftarrow 0$ ;
5:   Generate  $\mathbf{s} \in \mathbb{R}^n$  by Equation (7);
6:   Update set:  $\mathbb{B}_\varphi^{\mathbf{P}} \leftarrow \mathbb{B}_\varphi^{\mathbf{P}} \cup \{\mathbf{s}\}$ ;
7:   for  $\theta_2 = \frac{2\pi}{\bar{q}_2} : \frac{2\pi}{\bar{q}_2} : (2\pi - \frac{2\pi}{\bar{q}_2})$  do
8:      $\vdots$ 
9:     for  $\theta_{n-1} = \frac{2\pi}{\bar{q}_{n-1}} : \frac{2\pi}{\bar{q}_{n-1}} : (2\pi - \frac{2\pi}{\bar{q}_{n-1}})$  do
10:      Generate  $\mathbf{s} \in \mathbb{R}^n$  by Equation (7);
11:      Update set:  $\mathbb{B}_\varphi^{\mathbf{P}} \leftarrow \mathbb{B}_\varphi^{\mathbf{P}} \cup \{\mathbf{s}\}$ ;
12:    end for
13:     $\vdots$ 
14:  end for
15: end for
16: for  $j = 1$  to  $p$  do ▷ Start training curriculum
17:   for  $\mathbf{s} \in \mathbb{B}_\varphi^{\mathbf{P}}$  do
18:    Set  $\mathbf{s}(1) \leftarrow \mathbf{s}$  for system in Equation (1);
19:    Train (test) Phy-DRL agent for one episode;
20:   end for
21: end for

```

by the solutions of worst-case samples in Equation (7). The number of samples n is a user-defined parameter to determine the sparsity of the samples. As shown in Section 4, we found that training on a few worst-case conditions can already learn a safe policy that renders the safety envelope invariant. In the training curriculum, we iteratively set the system's state at the generated worst-case conditions. This can help the agent to sufficiently visit the challenging conditions for learning a safe and robust policy.

Episode Complexity. Line 3, Line 7 and Line 9 indicate the sampling number of each radian θ_r is $q_r - 1$, where $r = 2, \dots, n-1$, while the number of θ_1 is q_n . This setting is because of the observation from Equation (7) that if $\theta_i = 0$, the values of radians $\theta_1, \dots, \theta_{i-1}$ have no influence on solution \mathbf{y} . For example, if we let $\theta_{n-1} = 0$, even without knowing $\theta_1, \dots, \theta_{n-2}$, the \mathbf{y} can be directly obtained as $\mathbf{y} = \sqrt{\frac{\varphi}{\lambda_1(\mathbf{P})}} [0, 0, \dots, 0, 1]^\top$. This observation motivates Line 4 of Algorithm 1. The total number of episodes (or sampled worst-case samples) is thus

$$\text{number of episodes} = q_1 \cdot p \cdot \prod_{i=2}^{n-1} (q_i - 1) + q_1 \cdot p. \quad (12)$$

4 Experiments

In this section, we evaluate the effectiveness of the proposed training algorithm using worst-case conditions and uniform sampled

conditions commonly used in literature [27, 32, 35]. We evaluate these two condition sampling strategy on simulated cart-pole system, a 2D quadrotor, and a quadruped robot, and we cite the following safety samples from [10] for defining safety metrics.

Internal-Envelope (IE) sample $\tilde{\mathbf{s}}$: (13)

if $\mathbf{s}(1) = \tilde{\mathbf{s}} \in \Omega$, then $\mathbf{s}(k) \in \Omega, \forall k \in \mathbb{N}$.

External-Envelope (EE) sample $\tilde{\mathbf{s}}$: (14)

if $\mathbf{s}(1) = \tilde{\mathbf{s}} \in \mathbb{X}$, then $\mathbf{s}(k) \in \mathbb{X} \setminus \Omega, \exists k \in \mathbb{N}$.

Intuitively, **IE** samples means that the system starts from the safety envelope and it always stay in the safety envelope. **EE** means that the system starts from the safety set but not in the safety envelope and always stays in the safety set.

4.1 DRL Policy Setup

We implement our policy using Phy-DRL framework [10], where the a_{drl} is implemented based on DDPG algorithm [31]. The action value function and actor network are both parameterized using a multi-layer-perceptions (MLP) model. The reward function is designed as the format of Equation (5), where the matrix \mathbf{P} and \mathbf{H} are obtained as in [9] by solving LMI problems for each robot using their own linear dynamics models.

Table 2: Training episodes and failed episodes for different period of training and numbers of sampled conditions. The failure episodes means the episode in which the system violates the safety constraints.

Sampling IDs	EPs Num	Failed Eps	Failure rate
worst-case (2-3)	30	3	10.0%
random (2-3)	30	29	96.67%
worst-case-w.t.(2-3)	30	9	29.0%
random-w.t. (2-3)	30	15	50.00%
worst-case (2-4)	80	3	3.75%
random (2-4)	80	74	92.5%
worst-case-w.t.(2-4)	80	0	0.0%
random-w.t. (2-4)	80	46	57.50%
worst-case (2-5)	170	1	0.59%
random (2-5)	170	154	90.6%
worst-case-w.t. (2-5)	170	0	0.0%
random-w.t.(2-5)	170	85	50.00%

4.2 Cart pole

In the cart pole case study, the objective is to learn a safe policy that stabilizes the pole from as many initial conditions as possible without violating safety constraints. For Algorithm 1, we let $p = 2$ and $q_1 = q_2 = q_3 = 5$, which leads to in total 170 episodes, calculated using (12). For the uniform sampling scheme, we let the initial position, velocity, angle, and angular velocity be uniformly sampled over the intervals $[-0.9, 0.9]$, $[-3.0, 3.0]$, $[-0.8, 0.8]$, and $[-4.5, 4.5]$, respectively. The bounds of intervals are the same as those of the safety envelope used for worst-case conditions generations. For training, the maximum length of one episode is 500

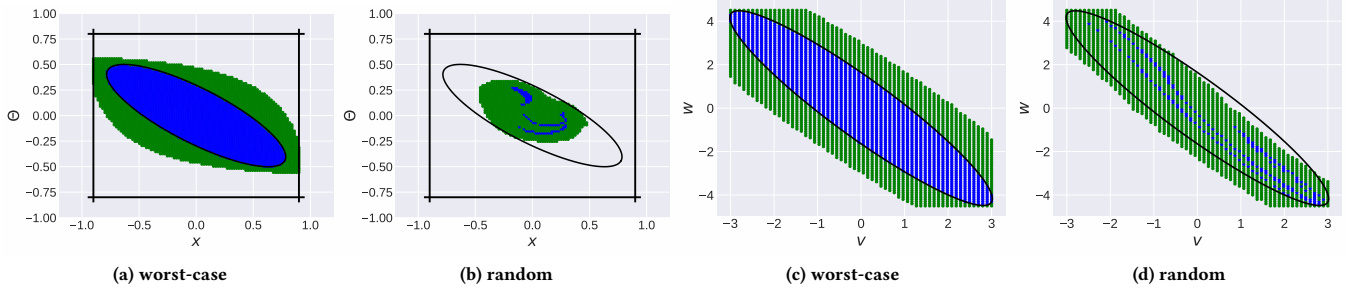


Figure 3: Worst-case Sampling vs. Random Sampling, with termination condition. Blue: area of IE samples (14). Green: area of EE samples (15). Ellipse area: safety envelope. The (a) and (b) are the testing result visualized on x and θ dimensions, where (c) and (d) are the results visualized on v and w dimensions. The size of colored area indicates the safety and robustness of the learned policy, the larger the better.

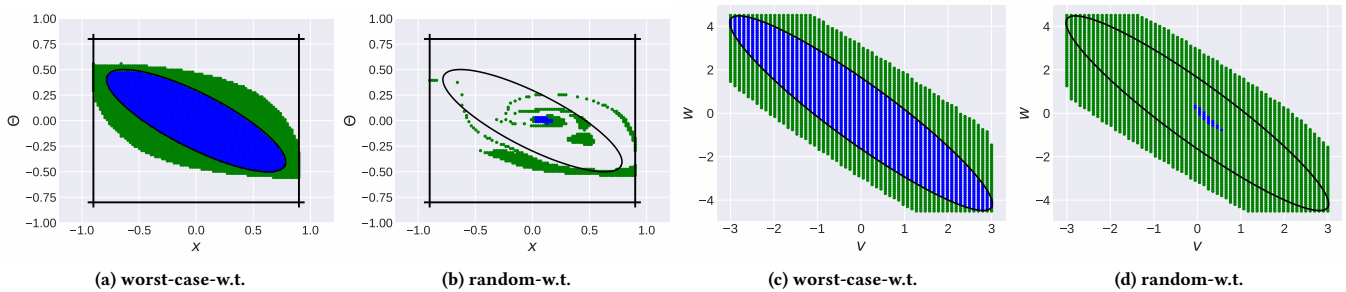


Figure 4: Worst-case Sampling vs. Random Sampling, without using termination condition in training.

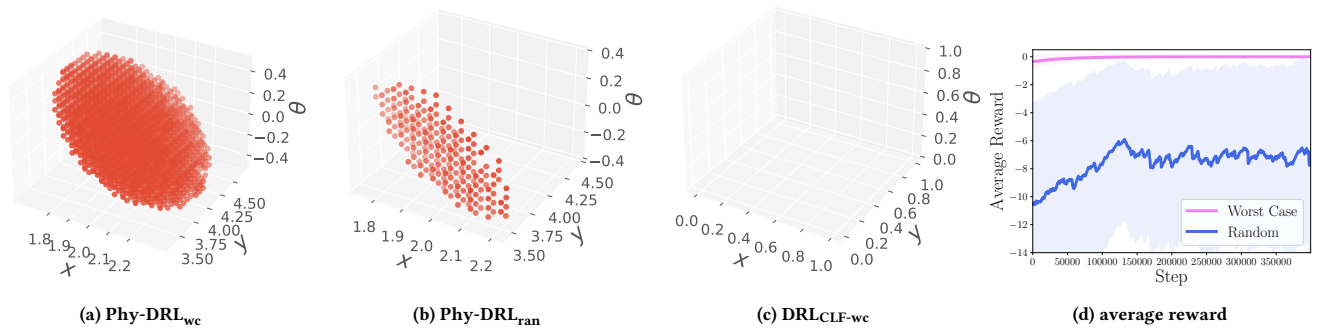


Figure 5: (a)-(c): The number and locations of IE samples (14) visualized in $x - y - \theta$ space. Phy-DRL_{wc} has much more colored points, meaning that it can almost render the safety envelope invariant. (d): Reward curves (five random seeds): Phy-DRL_{wc} v.s. Phy-DRL_{ran} .

steps. Additionally, we introduce a terminal condition to the training episode that stops the system from running when a violation of safety occurs in training: $\hat{\gamma} = 1$ if $|x(k)| \geq 0.9$ or $|\theta(k)| \geq 0.8$, and 0, otherwise. Summarily, we reset episodes if the maximum step of system running is reached, or $\hat{\gamma} = 1$.

We consider four sampling methods for Phy-DRL training. They are named 1) ‘worst-case’ (i.e., Algorithm 1 with termination condition), 2) ‘random’ (i.e., random sampling with termination condition), 3) ‘worst-case-w.t.’ (i.e., Algorithm 1 without termination condition), and 4) ‘random-w.t.’ (i.e., random sampling without termination condition).

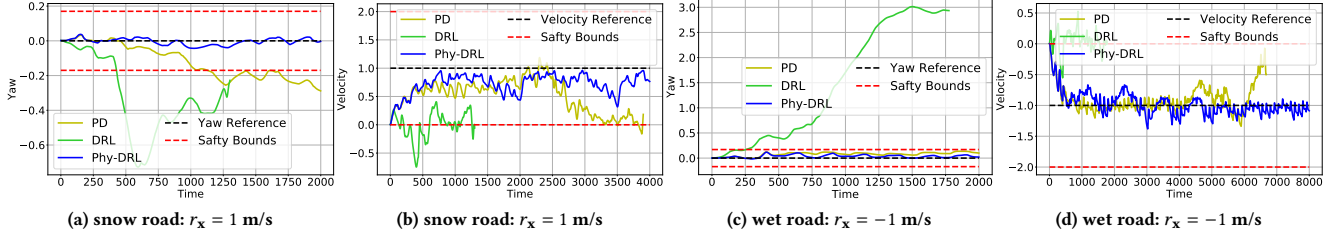


Figure 6: Yaw and velocity trajectories under velocity commands $r_x = -1$ or 1 m/s on snow and wet road.

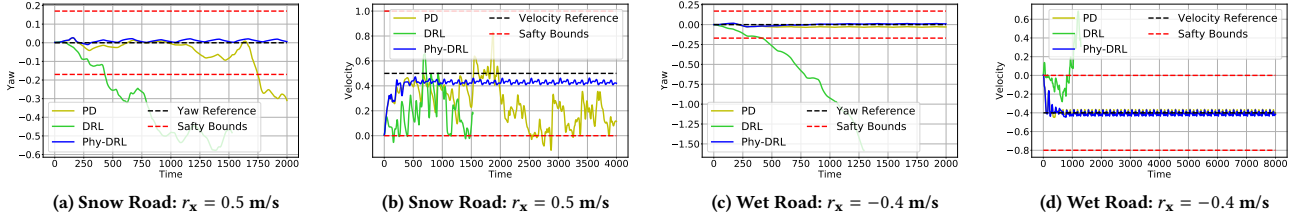


Figure 7: Yaw and velocity trajectories under velocity commands $r_x = 0.5$ or -0.4 m/s on snow and wet road.

We use the areas of IE sample (14) and EE sample (15) as the safety metrics. During testing, we intentionally introduce random friction force to the system to increase the testing variety, therefore to showcase the robustness of the learned policy. The sample areas of policies trained by the worst-case sampling and random sampling schemes with the episode termination condition are shown in Figure 3. The sample areas of policies trained without the episode termination condition are shown in Figure 4. For each training episode, if the system violates the safety constraint (2), this episode is marked as a failed episode. Table 2 summarizes the number of failed episodes and the failure rate of the four sampling schemes. Observing Figure 3, Figure 4, and Table 2, we discover:

- The worst-case sampling procedure (i.e., Algorithm 1) empowers the Phy-DRL with fast and efficient training towards a safety guarantee for both **with** and **without** the episode termination settings, i.e., the learned policy successfully rendering the safety envelope invariant (see Figure 3 (a) and (c), and Figure 4 (a) and (c)).
- Compared with random sampling, the worst-case sampling has much smaller failure rate of episodes (see last two columns in Table 2). The root reason goes back to the solutions of worst-case samples in Lemma 3.2, which automatically avoids many samples that are physically infeasible to control. Meanwhile, the safety areas of action policy trained using random sampling are much smaller (see Figure 3 (b) and (d), and Figure 4 (b) and (d)).

Moreover, we are interested in how many worst-cases and training period are needed for learning a robust safe policy. Therefore, we consider two additional settings: (2-3) denoting $p = 2$ and $q_1 = q_2 = q_3 = 3$ and (2-4) denoting $p = 2$ and $q_1 = q_2 = q_3 = 4$. All other settings are identical to the experiments in Section 4.2. For those two settings, the areas of IE and EE samples of action

policies trained under the worst-case sampling and random sampling schemes are shown in Figure 8 and Figure 9, respectively. Meanwhile, Table 2 summarizes the number of failed episodes and the failure rate of the four sampling schemes. It can be seen from Table 2, the number of failed episodes for worst-case training is consistently less than the random condition training. As demonstrated in Figure 8, Figure 9, by training using few conditions, the Phy-DRL can already learn a safe policy. Another reason is that the build-in model based policy in Phy-DRL can efficiently guide the exploration of the policy. We also note from Table 2, the number of failed episodes for worst-case condition is very small but not very consistent. We attribute this to the randomness of the exploratory action during policy learning.

4.3 2D Quadrotor

In this case study, we use the 2D quadrotor simulator provided in Safe-Control-Gym [47] as an experimental system. It is characterized by (x, z) – the translation position of the CoM of the quadrotor in the xz -plane, θ – the pitch angle, and their velocities $v_x = \dot{x}$, $v_z = \dot{z}$, and $v_\theta = \dot{\theta}$. The mission of the action policy is to stabilize the quadrotor at the waypoint (r_x, r_z, r_θ) under safety constraints:

$$|x - r_x| \leq 0.5 \text{ m}, |z - r_z| \leq 0.8 \text{ m}, |\theta - r_\theta| \leq 0.8 \text{ rad}. \quad (15)$$

In this experiment, we set the training episode as 400 with the same episode length as 500. For comparison, we train three policies: Phy-DRL_{wc}, Phy-DRL_{ran}, and DRL_{CLF-wc}, denoting trained Phy-DRL policies using worst-case sampling, random sampling, and pure data-driven DRL policy trained using worst-case sampling and CLF-like reward (proposed in [44]), respectively. For the random sampling, we let the initial $x, z, \theta, v_x, v_z, v_\theta$ be uniformly sampled over the intervals $[1.5, 2.5]$, $[3.2, 4.8]$, $[-0.8, 0.8]$, $[-1, 1]$, $[-10, 10]$,

and $[-45, 45]$, respectively. The intervals' bounds are the same as those of the safety envelope used for worst-case sampling.

For testing, we set initial velocities as zeros. The IE samples (14) of considered three policies are shown in Figure 5 (a)-(c). It can be seen from Figure 5, that Phy-DRL – powered by worst-case sampling – features much more stable and fast training towards safety guarantee. Meanwhile, the reward's training curves (five random seeds) of Phy-DRL_{wc} v.s. Phy-DRL_{ran} are shown in Figure 5 (d), where the training from the random conditions cause the large variance for policy learning. This could lead the policy to be sub-optimal, as also observed in [34].

At the last, DRL_{CLF-wc} has zero IE sample given the current training episodes. This suggests equipping DRL with only a worst-case sampling scheme cannot efficiently search for a safe action policy, and it needs a guide policy as in Phy-DRL [9] or more training steps.

4.4 Quadruped Robot

Section 4.2 and Section 4.3 have focused on safety performance; thus, this section focuses on robustness evaluation of safe policy in quadruped locomotion. The mission of the action policies includes safe lane tracking along the x-axis and safe velocity regulation. We consider the following safety constraints:

$$\begin{aligned} |\text{yaw}| &\leq 0.17 \text{ rad}, |\text{CoM x-velocity} - r_x| \leq |r_x|, \\ |\text{CoM z-height} - 0.24 \text{ m}| &\leq 0.13 \text{ m}, \end{aligned} \quad (16)$$

where r_x denotes velocity reference or command. The model-based design follows [10]. We train and evaluate the policy in Pybullet simulator with varying road conditions. For the worst-case training, we consider only one worst-case sample: forward velocity command $r_x = 1$ m/s and snow road (low friction on terrain). We perform comparisons with the other two models: proportional-derivative (PD) controller developed in [15] and pure data-driven DRL policy [31]. The Phy-DRL with the worst-case sampling is trained for only 10^6 steps, while the pure data-driven DRL is trained for 10^7 steps.

We also consider a testing environment very different from a training environment: backward velocity command $r_x = -1$ m/s and wet road. The yaw and CoM-velocity trajectories are shown in Figure 6. In addition, another groups of experimental results for forward velocity command $r_x = 0.5$ m/s and snow road, and backward velocity command $r_x = -0.4$ m/s and wet road are shown in Figure 7. From Figure 6, Figure 7, we can see that compared with DRL and PD, the Phy-DRL's action policy (trained using only one worst-case sample) has much higher tracking performance under different road conditions while strictly following the safety regulations in Equation (17).

After training in the simulation, we also transferred the learned policy to the real robot; see a demonstration video available at [anonymous link](#). We note that crossing the white lane in the video means violating the first safety regulation (i.e. $|\text{yaw}| \leq 0.17$ rad) in Equation (17). We also note that the video does not include pure data-driven DRL policy as we found that DRL policy can not make progress after training 10^7 steps from scratch.

5 Conclusion and Discussion

This paper proposes the sparse worst-case sampling for Phy-DRL training. The particular design aims of worst-case sampling include i) automatically avoiding state samples that are physically infeasible and ii) focusing the training on corner cases represented by worst-case samples. The sparse worst-case sampling makes the Phy-DRL features much more efficient and fast training towards safety guarantee.

Under worst-case sampling, a potential negative issue could be increased instability of the model-based policy in Phy-DRL, when training starts from boundary. To address this, Phy-DRL shall run on a fault-tolerant software architecture called Simplex [41]. In Simplex, we use the Phy-DRL as the complex and high-performance controller, which may have unknown defects. Meanwhile, Simplex's high-assurance controller (HAC) is function-reduced and simplified but verified, and it only guarantees the system's basic stable and safe operations. HAC is thus complementary to Phy-DRL and coordinated by a monitor. For example, the monitor triggers the switch from Phy-DRL to HAC once the real-time system states (under the control of Phy-DRL) leave the safety envelope. In other words, the HAC takes over at the cost of lower performance. When the system returns to the safety set, the Phy-DRL can be restarted and control can be retaken.

References

- [1] [n. d.]. AI INCIDENT DATABASE. <https://incidentdatabase.ai/entities/>.
- [2] Joshua Achiam, David Held, Aviv Tamar, and Pieter Abbeel. 2017. Constrained policy optimization. In *International conference on machine learning*. PMLR, 22–31.
- [3] Felix Berkenkamp, Matteo Turchetta, Angela Schoellig, and Andreas Krause. 2017. Safe model-based reinforcement learning with stability guarantees. *Advances in Neural Information Processing Systems* 30 (2017).
- [4] Rajendra Bhatia. 2009. *Positive definite matrices*. Princeton university press.
- [5] Daniel Bogdoll, Jasmin Breitenstein, Florian Heidecker, Maarten Bieshaar, Bernhard Sick, Tim Fingscheidt, and Marius Zöllner. 2021. Description of corner cases in automated driving: Goals and challenges. In *Proceedings of the IEEE/CVF International Conference on Computer Vision*. 1023–1028.
- [6] Joshua Bote. 2023. Waymo driverless car brings San Francisco traffic to a halt during rush hour. <https://www.sfgate.com/bayarea/article/waymo-rush-hour-traffic-standstill-17739556.php>. (2023).
- [7] Stephen Boyd, Laurent El Ghaoui, Eric Feron, and Venkataramanan Balakrishnan. 1994. *Linear matrix inequalities in system and control theory*. SIAM.
- [8] Yihao Cai, Hongpeng Cao, Yanbing Mao, Lui Sha, and Marco Caccamo. 2024. Simplex-enabled Safe Continual Learning Machine. *arXiv preprint arXiv:2409.05898* (2024).
- [9] Hongpeng Cao, Yanbing Mao, Lui Sha, and Marco Caccamo. 2023. Physics-Model-Regulated Deep Reinforcement Learning towards Safety & Stability Guarantees. In *62nd IEEE Conference on Decision and Control*. 8300–8305.
- [10] Hongpeng Cao, Yanbing Mao, Lui Sha, and Marco Caccamo. 2024. Physics-Regulated Deep Reinforcement Learning: Invariant Embeddings. In *The Twelfth International Conference on Learning Representations*. <https://openreview.net/forum?id=5Dwqu5urz5>
- [11] Ya-Chien Chang and Sicun Gao. 2021. Stabilizing neural control using self-learned almost Lyapunov critics. In *2021 IEEE International Conference on Robotics and Automation*. IEEE, 1803–1809.
- [12] Richard Cheng, Gábor Orosz, Richard M Murray, and Joel W Burdick. 2019. End-to-end safe reinforcement learning through barrier functions for safety-critical continuous control tasks. In *Proceedings of the AAAI conference on artificial intelligence*, Vol. 33. 3387–3395.
- [13] Richard Cheng, Abhinav Verma, Gabor Orosz, Swarat Chaudhuri, Yisong Yue, and Joel Burdick. 2019. Control regularization for reduced variance reinforcement learning. In *International Conference on Machine Learning*. 1141–1150.
- [14] Arthur Clavière, Eric Asselin, Christophe Garion, and Claire Pagetti. 2021. Safety Verification of Neural Network Controlled Systems. In *Proceedings of 51st Annual IEEE/IFIP International Conference on Dependable Systems and Networks Workshops*. 47–54.
- [15] Xingye Da, Zhaoming Xie, David Hoeller, Byron Boots, Anima Anandkumar, Yuke Zhu, Buck Babich, and Animesh Garg. 2021. Learning a contact-adaptive

- controller for robust, efficient legged locomotion. In *Conference on Robot Learning*. PMLR, 883–894.
- [16] Scott Fujimoto, Herke Hoof, and David Meger. 2018. Addressing function approximation error in actor-critic methods. In *International conference on machine learning*. PMLR, 1587–1596.
- [17] Pascal Gahinet, Arkadii Nemirovskii, Alan J Laub, and Mahmoud Chilali. 1994. The LMI control toolbox. In *Proceedings of 1994 33rd IEEE conference on decision and control*, Vol. 3. IEEE, 2038–2041.
- [18] Siddhant Gangapurwala, Alexander Mitchell, and Ioannis Havoutis. 2020. Guided constrained policy optimization for dynamic quadrupedal robot locomotion. *IEEE Robotics and Automation Letters* 5, 2 (2020), 3642–3649.
- [19] Zhenglei He, Kim-Phuc Tran, Sebastien Thomassey, Xianyi Zeng, Jie Xu, and Changhai Yi. 2021. A deep reinforcement learning based multi-criteria decision support system for optimizing textile chemical process. *Computers in Industry* 125 (2021), 103373.
- [20] Sandy H. Huang, Nicolas Papernot, Ian J. Goodfellow, Yan Duan, and Pieter Abbeel. 2017. Adversarial Attacks on Neural Network Policies. In *5th International Conference on Learning Representations, ICLR 2017, Workshop Track Proceedings*. <https://openreview.net/forum?id=ryvlRyBKI>
- [21] Laura Humphrey, Bettina Könighofer, Robert Könighofer, and Ufuk Topcu. 2016. Synthesis of Admissible Shields. In *Hardware and Software: Verification and Testing, Lecture Notes in Computer Science*. Springer, 134–151. https://doi.org/10.1007/978-3-319-49052-6_9 arXiv:1904.06938v1 [cs.LO]
- [22] Julian Ibarz, Jie Tan, Chelsea Finn, Mrinal Kalakrishnan, Peter Pastor, and Sergey Levine. 2021. How to train your robot with deep reinforcement learning: lessons we have learned. *The International Journal of Robotics Research* 40, 4-5 (2021), 698–721.
- [23] Tobias Johannink, Shikhar Bahl, Ashvin Nair, Jianlan Luo, Avinash Kumar, Matthias Loskyll, Juan Aparicio Ojea, Eugen Solowjow, and Sergey Levine. 2019. Residual reinforcement learning for robot control. In *2019 International Conference on Robotics and Automation (ICRA)*. IEEE, 6023–6029.
- [24] Guy Katz, Clark Barrett, David L Dill, Kyle Julian, and Mykel J Kochenderfer. 2017. Reluplex: An efficient SMT solver for verifying deep neural networks. In *Computer Aided Verification: 29th International Conference, CAV 2017*. Springer, 97–117.
- [25] Alex Kendall, Jeffrey Hawke, David Janz, Przemyslaw Mazur, Daniele Reda, John-Mark Allen, Vinh-Dieu Lam, Alex Bewley, and Amar Shah. 2019. Learning to drive in a day. In *2019 International Conference on Robotics and Automation*. IEEE, 8248–8254.
- [26] B Ravi Kiran, Ibrahim Sobh, Victor Talpaert, Patrick Mannion, Ahmad A Al Sallab, Senthil Yogamani, and Patrick Pérez. 2021. Deep reinforcement learning for autonomous driving: A survey. *IEEE Transactions on Intelligent Transportation Systems* 23, 6 (2021), 4909–4926.
- [27] Robert Kirk, Amy Zhang, Edward Grefenstette, and Tim Rocktäschel. 2023. A survey of zero-shot generalisation in deep reinforcement learning. *Journal of Artificial Intelligence Research* 76 (2023), 201–264.
- [28] Sergey Levine, Chelsea Finn, Trevor Darrell, and Pieter Abbeel. 2016. End-to-end training of deep visuomotor policies. *The Journal of Machine Learning Research* 17, 1 (2016), 1334–1373.
- [29] Jingqi Li, David Fridovich-Keil, Somayeh Sojoudi, and Claire J Tomlin. 2021. Augmented lagrangian method for instantaneously constrained reinforcement learning problems. In *2021 60th IEEE Conference on Decision and Control (CDC)*. IEEE, 2982–2989.
- [30] Tongxin Li, Ruixiao Yang, Guannan Qu, Yiheng Lin, Steven Low, and Adam Wierman. [n. d.]. Equipping Black-Box Policies with Model-Based Advice for Stable Nonlinear Control. *arXiv preprint* <https://arxiv.org/pdf/2206.01341.pdf>.
- [31] Timothy P. Lillicrap, Jonathan J. Hunt, Alexander Pritzel, Nicolas Heess, Tom Erez, Yuval Tassa, David Silver, and Daan Wierstra. 2016. Continuous control with deep reinforcement learning. In *4th International Conference on Learning Representations, ICLR*.
- [32] Minghuan Liu, Menghui Zhu, and Weinan Zhang. 2022. Goal-conditioned reinforcement learning: Problems and solutions. *arXiv preprint arXiv:2201.08299* (2022).
- [33] Bernard Marr. 2021. How Tesla Is Using Artificial Intelligence to Create The Autonomous Cars Of The Future. *Bernard Marr & Co*. <https://bernardmarr.com/how-tesla-is-using-artificial-intelligence-to-create-the-autonomous-cars-of-the-future/>.
- [34] Bhairav Mehta, Manfred Diaz, Florian Golemo, Christopher J Pal, and Liam Paull. 2020. Active domain randomization. In *Conference on Robot Learning*. PMLR, 1162–1176.
- [35] Fabio Muratore, Fabio Ramos, Greg Turk, Wenhao Yu, Michael Gienger, and Jan Peters. 2022. Robot learning from randomized simulations: A review. *Frontiers in Robotics and AI* 9 (2022), 799893.
- [36] NHTSA. [n. d.]. Summary Report: Standing General Order on Crash Reporting for Level 2 Advanced Driver Assistance Systems. *National Highway Traffic Safety Administration* [n. d.]. <https://www.nhtsa.gov/sites/nhtsa.gov/files/2022-06/ADAS-L2-SGO-Report-June-2022.pdf>
- [37] Theodore J Perkins and Andrew G Barto. 2002. Lyapunov design for safe reinforcement learning. *Journal of Machine Learning Research* 3, Dec (2002), 803–832.
- [38] Krishan Rana, Vibhavari Dasagi, Jesse Haviland, Ben Talbot, Michael Milford, and Niko Sünderhauf. [n. d.]. Bayesian controller fusion: Leveraging control priors in deep reinforcement learning for robotics. *arXiv preprint* <https://arxiv.org/pdf/2107.09822.pdf>.
- [39] Remo Sasso, Michelangelo Conserva, and Paulo Rauber. 2023. Posterior Sampling for Deep Reinforcement Learning. *The Fortieth International Conference on Machine Learning* (2023), 1–19.
- [40] Thomas Savage, Dongda Zhang, Max Mowbray, and Ehecatl Antonio Del Río Chanona. 2021. Model-free safe reinforcement learning for chemical processes using Gaussian processes. *IFAC-PapersOnLine* 54, 3 (2021), 504–509.
- [41] Lui Sha et al. 2001. Using simplicity to control complexity. *IEEE Software* 18, 4 (2001), 20–28.
- [42] Tian Tolentino. 2019. Autonomous aircraft market worth USD 23.7bn by 2030. <https://www.traveldailymedia.com/autonomous-aircraft-marke>.
- [43] Akifumi Wachi and Yanan Sui. 2020. Safe reinforcement learning in constrained Markov decision processes. In *International Conference on Machine Learning*. 9797–9806.
- [44] Tyler Westenbroek, Fernando Castaneda, Ayush Agrawal, Shankar Sastry, and Koushil Sreenath. 2022. Lyapunov Design for Robust and Efficient Robotic Reinforcement Learning. *arXiv:2208.06721* (2022). <https://arxiv.org/pdf/2208.06721.pdf>
- [45] Weiming Xiang, Patrick Musau, Ayana A Wild, Diego Manzananas Lopez, Nathaniel Hamilton, Xiaodong Yang, Joel Rosenfeld, and Taylor T Johnson. 2018. Verification for machine learning, autonomy, and neural networks survey. *arXiv preprint arXiv:1810.01989* (2018).
- [46] Ruihan Yang, Minghao Zhang, Nicklas Hansen, Huazhe Xu, and Xiaolong Wang. 2022. Learning vision-guided quadrupedal locomotion end-to-end with cross-modal transformers. *2022 International Conference on Learning Representations* (2022).
- [47] Zhaocong Yuan, Adam W Hall, Siqi Zhou, Lukas Brunke, Melissa Greeff, Jacopo Panerati, and Angela P Schoellig. 2022. Safe-control-gym: A unified benchmark suite for safe learning-based control and reinforcement learning in robotics. *IEEE Robotics and Automation Letters* 7, 4 (2022), 11142–11149.
- [48] Arnold Zachary and Toner Helen. 2021. AI Accidents: An Emerging Threat. *Center for Security and Emerging Technology* (2021). <https://doi.org/10.51593/20200072>
- [49] Liqun Zhao, Konstantinos Gatsis, and Antonis Papachristodoulou. 2023. Stable and Safe Reinforcement Learning via a Barrier-Lyapunov Actor-Critic Approach. In *62nd IEEE Conference on Decision and Control*. IEEE, 1320–1325.
- [50] Bingzhuo Zhong, Hongpeng Cao, Majid Zamani, and Marco Caccamo. 2023. Towards safe ai: Sandboxing dnns-based controllers in stochastic games. In *Proceedings of the AAAI Conference on Artificial Intelligence*, Vol. 37. 15340–15349.
- [51] Chris Ziegler. 2016. A Google self-driving car caused a crash for the first time. <https://www.theverge.com/2016/2/29/11134344/google-self-driving-car-crash-report>

A Appendix

A.1 Auxiliary Lemmas

Lemma A.1 (Positive Definiteness [4]). *A matrix $\mathbf{A} \in \mathbb{R}^{n \times n}$ is called positive definite if it is symmetric and all its eigenvalues are positive. In other words, there exists an orthogonal matrix $\mathbf{Q} \in \mathbb{R}^{n \times n}$, such that*

$$\mathbf{Q}^\top \cdot \mathbf{A} \cdot \mathbf{Q} = \begin{bmatrix} \lambda_1 & 0 & \cdots & 0 \\ 0 & \lambda_2 & \cdots & 0 \\ \vdots & \vdots & \ddots & \vdots \\ 0 & 0 & \cdots & \lambda_n \end{bmatrix}, \quad (17)$$

with $\lambda_1 > 0, \lambda_2 > 0, \dots, \lambda_n > 0$.

A.2 Proof of Lemma 3.2

The $\mathbf{P} > 0$ means the matrix \mathbf{P} is positive definite. In light of Lemma A.1 in Appendix A.1, there exists an orthogonal matrix $\mathbf{Q}(\mathbf{P}) \in \mathbb{R}^{n \times n}$, such that

$$\mathbf{Q}^\top(\mathbf{P}) \cdot \mathbf{P} \cdot \mathbf{Q}(\mathbf{P}) = \underbrace{\begin{bmatrix} \lambda_1(\mathbf{P}) & 0 & \cdots & 0 \\ 0 & \lambda_2(\mathbf{P}) & \cdots & 0 \\ \vdots & \vdots & \ddots & \vdots \\ 0 & 0 & \cdots & \lambda_n(\mathbf{P}) \end{bmatrix}}_{\triangleq \Lambda(\mathbf{P})}, \quad (18)$$

$$\text{with } \lambda_1(\mathbf{P}) > 0, \lambda_2(\mathbf{P}) > 0, \dots, \lambda_n(\mathbf{P}) > 0. \quad (19)$$

Considering Equation (19), the $\mathbf{s}^\top \cdot \mathbf{P} \cdot \mathbf{s} = \varphi$ equates to

$$\mathbf{s}^\top \cdot \mathbf{P} \cdot \mathbf{s} = \mathbf{s}^\top \cdot \mathbf{Q}(\mathbf{P}) \cdot \Lambda(\mathbf{P}) \cdot \mathbf{Q}^\top(\mathbf{P}) \cdot \mathbf{s} = \varphi, \quad (20)$$

whose transformation utilizes a well-known property of orthogonal matrix: $\mathbf{Q}^\top(\mathbf{P}) = \mathbf{Q}^{-1}(\mathbf{P})$.

Let us define $\mathbf{y} \triangleq \mathbf{Q}^\top(\mathbf{P}) \cdot \mathbf{s}$. Recalling the $\Lambda(\mathbf{P})$ defined in Equation (19), Equation (20) equivalently transforms to

$$\sum_{i=1}^n \frac{\lambda_i(\mathbf{P})}{\varphi} \cdot y_i^2 = 1. \quad (21)$$

We next use the mathematical induction to prove that Equation (7) is the solution to the problem in Equation (21). To complete this proof task, we first let $n = 2$. In this case, we observe from Equation (7) that

$$[y]_1 = \sqrt{\frac{\varphi}{\lambda_1(\mathbf{P})}} \cdot \sin(\theta_1), \quad [y]_2 = \sqrt{\frac{\varphi}{\lambda_2(\mathbf{P})}} \cdot \cos(\theta_1),$$

which, in conjunction with the well-know triple angle identity $\sin^2(\theta_1) + \cos^2(\theta_1) = 1$, directly leads to the formula in Equation (21) with $n = 2$. We then consider the case of $n = p > 2$. Assuming Equation (7) is the solution to the problem in Equation (21) with $n = p$, we have

$$\sum_{i=1}^p \frac{\lambda_i(\mathbf{P})}{\varphi} \cdot \bar{y}_i^2 = 1, \quad (22)$$

where

$$[\bar{y}]_i \triangleq \begin{cases} \sqrt{\frac{\varphi}{\lambda_1(\mathbf{P})}} \cdot \sin(\theta_1) \cdot \prod_{m=2}^{p-1} \sin(\theta_m), & i = 1 \\ \sqrt{\frac{\varphi}{\lambda_i(\mathbf{P})}} \cdot \cos(\theta_{i-1}) \cdot \prod_{m=i}^{p-1} \sin(\theta_m), & i \geq 2 \end{cases}. \quad (23)$$

Based on this observation, we need to prove that Equation (7) is the solution to the problem in Equation (21) with $n = p + 1$. For the $n = p + 1$ and $\mathbf{y} \in \mathbb{R}^{p+1}$, according to Equation (7) to have

$$[y]_i \triangleq \begin{cases} \sqrt{\frac{\varphi}{\lambda_1(\mathbf{P})}} \cdot \sin(\theta_1) \cdot \prod_{m=2}^p \sin(\theta_m), & i = 1 \\ \sqrt{\frac{\varphi}{\lambda_i(\mathbf{P})}} \cdot \cos(\theta_{i-1}) \cdot \prod_{m=i}^p \sin(\theta_m), & i \geq 2 \end{cases}$$

which is equivalent to

$$[y]_i \triangleq \begin{cases} \sqrt{\frac{\varphi}{\lambda_1(\mathbf{P})}} \cdot \sin(\theta_1) \cdot \prod_{m=2}^{p-1} \sin(\theta_m) \cdot \sin(\theta_p), & i = 1 \\ \sqrt{\frac{\varphi}{\lambda_i(\mathbf{P})}} \cdot \cos(\theta_{i-1}) \cdot \prod_{m=i}^{p-1} \sin(\theta_m) \cdot \sin(\theta_p), & 2 \leq i \leq p \\ \sqrt{\frac{\varphi}{\lambda_{p+1}(\mathbf{P})}} \cdot \cos(\theta_p), & i = p + 1 \end{cases}. \quad (24)$$

Observing Equation (24) and Equation (22) with its solution in Equation (23), we have

$$\begin{aligned} \sum_{i=1}^{p+1} \frac{\lambda_i(\mathbf{P})}{\varphi} \cdot y_i^2 &= \sum_{i=1}^p \frac{\lambda_i(\mathbf{P})}{\varphi} \cdot y_i^2 + \frac{\lambda_{p+1}(\mathbf{P})}{\varphi} \cdot y_{p+1}^2 \\ &= \sin^2(\theta_p) \cdot \sum_{i=1}^p \frac{\lambda_i(\mathbf{P})}{\varphi} \cdot \bar{y}_i^2 + \frac{\lambda_{p+1}(\mathbf{P})}{\varphi} \cdot y_{p+1}^2 \\ &= \sin^2(\theta_p) + \cos^2(\theta_p) = 1, \end{aligned} \quad (25)$$

by which we can conclude that Equation (24) is the solution to Equation (21) with $n = p + 1$. Hereto, we can conclude that the formula in Equation (7) solves the problem in Equation (21).

We are finally, recalling the definition of an orthogonal matrix, i.e., $\mathbf{Q}(\mathbf{P}) \cdot \mathbf{Q}^{-1}(\mathbf{P}) = \mathbf{Q}(\mathbf{P}) \cdot \mathbf{Q}^\top(\mathbf{P}) = \mathbf{I}_n$, we can directly obtain Equation (7) from the notation $\mathbf{y} \triangleq \mathbf{Q}^\top(\mathbf{P}) \cdot \mathbf{s}$.

A.3 Ablation study

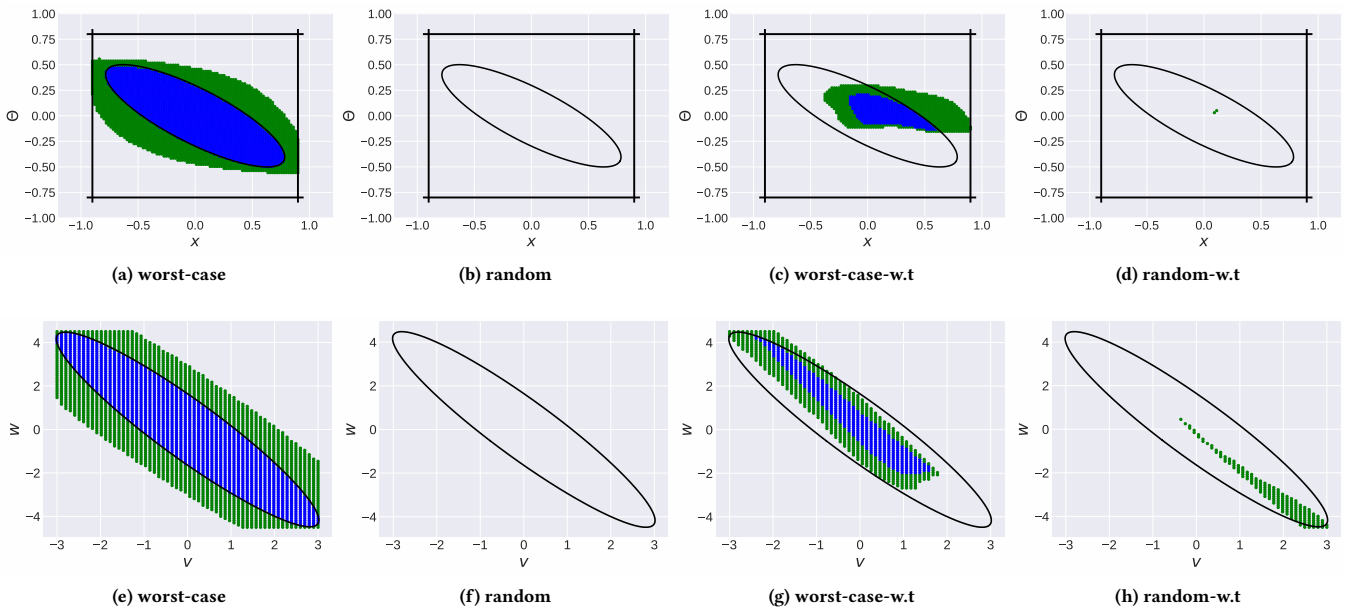


Figure 8: (2-3) Worst-case Sampling vs. Random Sampling, with and without termination condition. Blue: area of IE samples. Green: area of EE samples. Ellipse area: safety envelope.

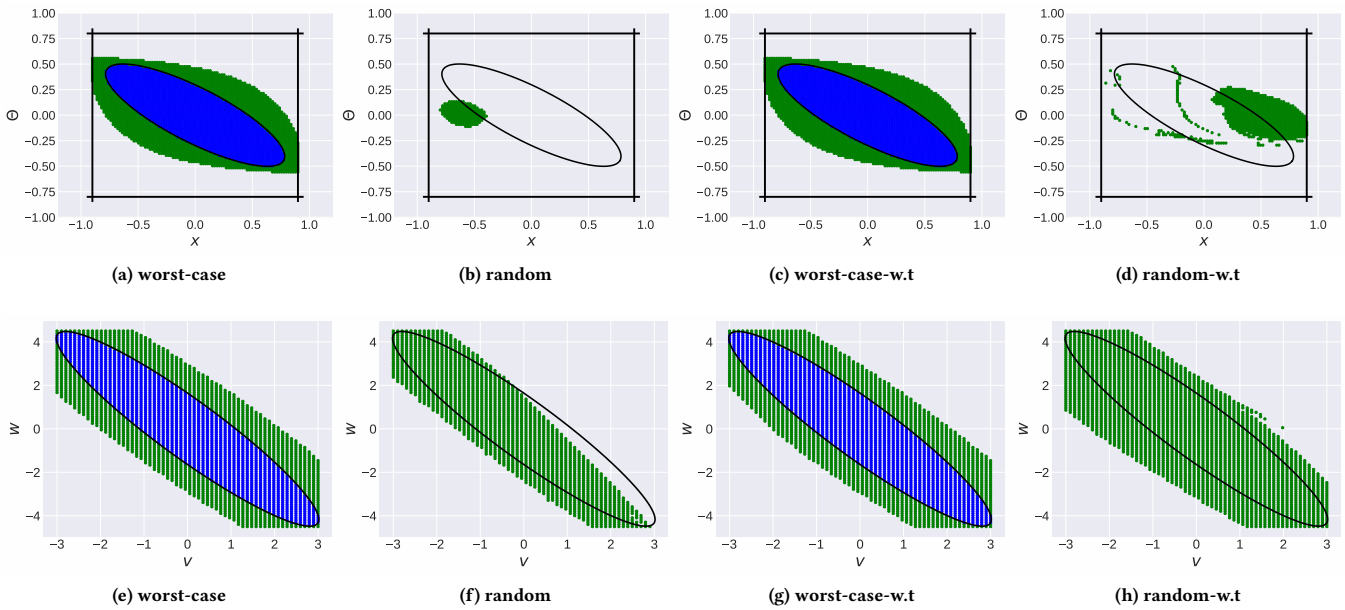


Figure 9: (2-4) Worst-case Sampling vs. Random Sampling, with and without termination condition. Blue: area of IE samples. Green: area of EE samples. Ellipse area: safety envelope.